Microwave Plasma Sintered Nanocrystalline Bi_2O_3−HfO_2−Y_2O_3 Composite Solid Electrolyte

Qiang Zhen,[†,§] Girish M. Kale,*[,‡] Weiming He,[§] and Jianqiang Liu[§]

Nano-science and Nano-technology Research Center, School of Materials Science and Engineering, Shanghai University, Shanghai 200444, P. R. China, Institute for Materials Research, University of Leeds, Leeds LS2 9JT, United Kingdom, and School of Materials Science and Engineering, Shanghai University, Shanghai 200072, P. R. China

Received May 22, 2006. Revised Manuscript Received October 24, 2006

Processing and characterization of nanocrystalline Bi_2O_3−HfO_2−Y_2O_3 composite solid electrolyte having high density and conductivity has been investigated and reported in this paper. Nanopowders of mixed bismuth oxide, hafnia, and yttrium oxide in Bi_2O_3:HfO_2:Y_2O_3 = 3:2:1 molar ratio have been prepared by a reverse titration chemical coprecipitation from Bi^{3+}, Hf^{4+}, and Y^{3+} containing aqueous solution. The high density, nanocrystalline Bi_2O_3−HfO_2−Y_2O_3 solid electrolyte has been synthesized by microwave plasma and pressureless sintering. From the XRD results, the growth behavior indicates that growth of both δ-Bi_2O_3 and c-HfO_2 crystallites obeys the parabolic rate law, expressed as $(D - D_0)^2 = kt$, during the sintering process. After the samples were sintered in microwave plasma at 700 °C for 30 min, the relative density was found to be greater than 96%. Moreover, the sintered specimens exhibit considerably finer microstructure and greater densification compared to that of samples sintered by conventional pressureless sintering. Results of AC impedance spectroscopy of the solid electrolyte indicates that the conductivity of nanocrystalline Bi_2O_3−HfO_2−Y_2O_3 electrolyte was more than 10^{-6} S cm^{-1} at 350 °C and 10^{-2} S cm^{-1} at 550 °C, which is significantly higher than that of microcrystalline HfO_2-based solid electrolyte.

1. Introduction

Functional ceramics based on stabilized δ-Bi_2O_3 phase with high oxide (O^{2-}) ion conductivity are promising solid electrolyte materials for solid oxide fuel cells (SOFC), high purity oxygen generators, and electrochemical sensors.[1−6] The oxide ion conductivity of microcrystalline Bi_2O_3-based solid electrolyte, e.g., Y_2O_3-doped Bi_2O_3, is several orders of magnitude higher than that of the corresponding ZrO_2-based material at temperatures below 800 °C.[7] HfO_2 has similar crystal structure and physical and chemical properties akin to ZrO_2. Compared to ZrO_2-based solid electrolyte, HfO_2-based solid electrolyte has superior mechanical properties and much lower limiting oxygen partial pressure for the onset of electronic conduction ($P_{e'} < 10^{-12}$ Pa) which implies that HfO_2-based solid electrolyte can exhibit high O^{2-} ion transference number at much lower oxygen partial pressure.[8] Therefore, a new dense nanocrystalline composite solid electrolyte in the Bi_2O_3−HfO_2−Y_2O_3 system is expected to have ionic conductivity superior to Y_2O_3-stabilized HfO_2 and mechanical properties superior Y_2O_3-stabilized Bi_2O_3.

Systematic investigations for the production and properties of nanocrystalline Bi_2O_3−HfO_2−Y_2O_3 solid electrolyte have been scanty although there is enough literature available on synthesis, densification, and measurement of physical as well as electrical properties of microcrystalline Bi_2O_3−Y_2O_3 ceramics and HfO_2−Y_2O_3-related ceramics.[1−10] Recently, nanopowders of materials containing Bi_2O_3 or HfO_2 have been prepared by using various methods, such as reverse chemical titration,[1] chemical precipitation,[11−13] sol−gel,[14] spontaneous combustion,[15] and solid-state reaction method.[16] The bulk density of sintered ceramics approaching close to the theoretical density could be easily achieved at fairly low temperatures when the particle size of the powders is in the

* Author e-mail for all correspondence: g.m.kale@leeds.ac.uk.
† Nano-science and Nano-technology Research Center, School of Materials Science and Engineering, Shanghai University.
‡ University of Leeds.
§ School of Materials Science and Engineering, Shanghai University.

(1) Zhen, Q.; Kale, G. M.; Li, R.; He, W. M.; Liu, J. Q. *Solid State Ionics* **2005**, *176*, 2727−2733.
(2) Doshi, R.; Richards, Von, L.; Carter, J. D.; Wang, X.; Krumpelt, M. *J. Electrochem. Soc.* **1999**, *146*, 1273−1278.
(3) Hirabayashi, D.; Hashimoto, A.; Hibino, T.; Harada, U.; Sano, M. *Electrochem. Solid State Lett.* **2004**, *7*, A108−A110.
(4) Asahara, S.; Michiba, D.; Hibino, M.; Yao, T. *Electrochem. Solid State Lett.* **2005**, *8*, A449−A451.
(5) Li, X.; Xiong, W.; Kale, G. M. *Electrochem. Solid-State Lett.* **2005**, *8*, H27−H30.
(6) Xiong, W.; Kale, G. M. *Sensors Actuators B* **2006**, *114*, 101−108.
(7) Watanabe, A.; Kikuchi, T. *Solid State Ionics* **1986**, *21*, 287−291.
(8) Wang, C. Z. *Solid Electrolyte and Chemical Sensors*; Metallurgical Industry Press: 2000.
(9) Karch, J.; Birringer, R.; Gleiter, H. *Nature* **1987**, *330*, 556−558.
(10) Ferrari, A. *Development, Industrialization of Nanocomposite Ceramic Material*, Proceedings of Nanostructure Materials and Coating '95, Atlanta, GA, 1995.
(11) Kruidhof, H.; Seshan Jr, K.; Lippens, B. C.; Gellings, P. J.; Burggraaf, A. J. *Materials Research Bulletin* **1987**, *22*, 1635−1643.
(12) Bhattacharya, A. K.; Mallick, K. K. *Solid State Communications* **1994**, *91*, 357−360.
(13) Hirano, T.; Namikawa, T. *IEEE. Transcations on Magnetics* **1999**, *35*, 3487−3489.
(14) Joshi, P. C.; Krupanidi, S. B. *J. Appl. Phys.* **1992**, *72*, 5827−5833.
(15) Zeng, Y.; Lin, Y. S. *J. Mater. Sci.* **2001**, *36*, 1271−1276.
(16) Li, W. Q.; Li, J.; Xia, X.; Chao, Y. L. *Acta. Chimica. Sinica*. **1999**, *57*, 491−495.

10.1021/cm061197i CCC: $37.00
Published on Web 12/16/2006

nanometer range compared to the conventional ceramic powders in submicron range.[13] Besides this, the nanostructured high-density compact also exhibits significantly improved mechanical properties.[14] Application of nanocrystalline ceramics can lead to the development of electrochemical devices that have considerably low operating temperatures and can exhibit significantly improved ionic conductivity.[10] Therefore, nanocrystalline $Bi_2O_3-HfO_2-Y_2O_3$ could be a promising solid electrolyte material for the fabrication of gas sensors for in-line monitoring of automotive emission, air-to-fuel ratio in automotive combustion process, designing planar fuel cells, and monitoring the atmospheric pollutants.

The fabrication of nanocrystalline $Bi_2O_3-HfO_2-Y_2O_3$ solid electrolyte involves two key steps: first the preparation of mixed nanopowders and second their transformation into nanocrystalline $Bi_2O_3-HfO_2-Y_2O_3$ solid electrolyte powder. Among the methods mentioned earlier for the synthesis of nanopowders of materials containing Bi_2O_3 or HfO_2, the chemical precipitation process incorporating surface modifiers has been one of the most effective methods for the preparation of nanopowders of functional ceramics. The nanopowders of functional ceramic materials can prove to be technologically useful if they are transformed into dense structures by sintering at elevated temperatures without allowing excessive grain growth. The main advantage of microwave plasma sintering process is that the process is rapid and can prevent excessive grain growth during sintering process in comparison to the other conventional sintering processes. Further, the coupling of microwave with the cations and anions in the ceramic materials during the heating process can appreciably enhance the mass transfer within the ceramic compact which can in turn influence the sintering and grain growth kinetics of the material compared to that observed in the conventional sintering processes of ceramic materials. There is a very limited understanding of the influence of microwave sintering process on the grain growth and kinetics of sintering process in ceramic materials due to the limited number of investigations in this area of research.

Hence, the present work has been focused on preparing mixed nanopowders of $Bi_2O_3+HfO_2+Y_2O_3$ by reverse chemical titration coprecipitation[1] and fabrication of dense nanocrystalline $Bi_2O_3-HfO_2-Y_2O_3$ solid electrolyte by a novel microwave plasma sintering process. The molar ratio of Bi_2O_3:HfO_2:Y_2O_3 = 3:2:1 is maintained for two main reasons, first to produce δ-Bi_2O_3 and c-HfO_2 single phases successfully in a composite and also to enable sintering of the composite solid electrolyte at lower temperatures with the assistance of δ-Bi_2O_3 acting as a sintering aid while c-HfO_2 acting as a toughening agent. In addition to this, the grain growth kinetics of δ-Bi_2O_3 and c-HfO_2, as well as the electrical properties of the dense nanocrystalline $Bi_2O_3-HfO_2-Y_2O_3$ solid electrolyte, have been measured in this study.

2. Experimental Methods

2.1. Sample Preparation. Mixed nanopowders of $Bi_2O_3-HfO_2-Y_2O_3$ in Bi_2O_3:HfO_2:Y_2O_3 = 3:2:1 molar ratio has been prepared by reverse chemical titration coprecipitation.[1] First, 550 mL of aqueous ammonia solution having a concentration of 1.26 mol/L and a pH ≈ 12 was prepared by mixing analytically pure aqueous ammonia and distilled water. The analytically pure $Bi(NO_3)_3{\cdot}5H_2O$, $HfOCl_2$ and $Y(NO_3)_3{\cdot}6H_2O$, in a molar ratio of 3:1:1, were dissolved in dilute nitric acid to prepare a nitrate solution containing a total metal ion (Bi^{3+}, Hf^{4+} and Y^{3+}) concentration of 0.125 mol/L. The 50 mL prepared nitrate solution was added dropwise into the aqueous ammonia solution in a reaction vessel at room temperature. The solution was continuously stirred using a magnetic needle and was maintained at pH ≈ 12. During the chemical titration, 1 wt.% PEG6000 (poly(ethylene glycol) of average molecular weight equal to 6000) dissolved in aqueous ammonia solution was added as a dispersing agent. The obtained suspension was further agitated in an ultrasonic bath to prevent any formation of agglomerates and was washed repeatedly with distilled water to washout all the chloride anions. The precipitate containing mixed hydroxide of Bi^{3+}, Hf^{4+}, and Y^{3+} was oven dried at 80 °C for 12 h and calcined at 700 °C for 1 h to yield mixed nanopowders of $Bi_2O_3-HfO_2-Y_2O_3$.

The mixed oxide nanopowders synthesized as above were pressed uniaxially into disk-shaped pellets having an outer diameter of 10 mm and a thickness of 2 mm at a relatively low pressure of 15 MPa. Approximately 3 wt.% polyvinyl alcohol (PVA) was used as a binder and a 20 wt.% stearic acid mixed with ethyl alcohol as a lubricant. The samples were sintered at temperature of 600, 700, and 800 °C in microwave plasma under oxygen atmosphere of 40 mmHg for different lengths of sintering time in order to study the microstructure development and grain growth kinetics. Figure 1 shows the schematic diagram of microwave plasma equipment used in this study. This equipment consists of microwave generator, microwave transmission and conversion system, gas control system, reaction chamber, vacuum system, and pressure monitor. In this work, the microwave power was maintained in the range of 0−1000 W at 2.45 GHz frequency. The samples' temperature was measured with an infrared optical temperature monitor. The reaction chamber consists of a quartz bell-jar (ϕ120 mm), quartz current equalizer, quartz platform (ϕ76 mm), and quartz sample holder. The samples were placed in the center of the quartz holder in order to keep them in the center of plasma during the sintering period so that the samples could be heated uniformly and rapidly by plasma.

Duplicate specimens were sintered by a conventional pressureless sintering process at the same temperature for comparison with the microwave plasma sintering process. The heating rate of all the samples during the sintering stage was maintained at 10 °C/min. After the selected time interval, the samples were withdrawn from the furnace and were allowed to cool naturally in ambient atmosphere.

2.2. Materials Characterization. The phases present in the calcined nanopowder and sintered samples were analyzed by X-ray diffraction (Rigaku D/max2550V) using Cu Kα radiation with a nickel filter at room temperature. The mean diameter of nanocrystalline grains was determined according to Scherrer formula, $t = 0.9\lambda/\beta \cos(\theta)$, from the X-ray diffraction peak width at half-maxima. The morphology of nanopowder and sintered samples were also determined using transmission electron microscopy (Hitachi H-800) and high-resolution scanning electron microscopy (JSM-6700F). The bulk density of the sintered specimens was measured at ambient temperature with an accuracy of 100 μg cm^{-3} using an electronic densimeter (SD-120L, Mirage JICC Co) that employed the Archimedes principle. In all cases, distilled water was used as an immersion medium.

AC impedance spectroscopy using a two-probe method with Ag electrodes was carried out using a PAR M273A frequency response analyzer over a frequency range of 0.01 Hz to 99 kHz. The frequency response analyzer was interfaced to a computer using ZPlot software. Due to the small sample impedances at high

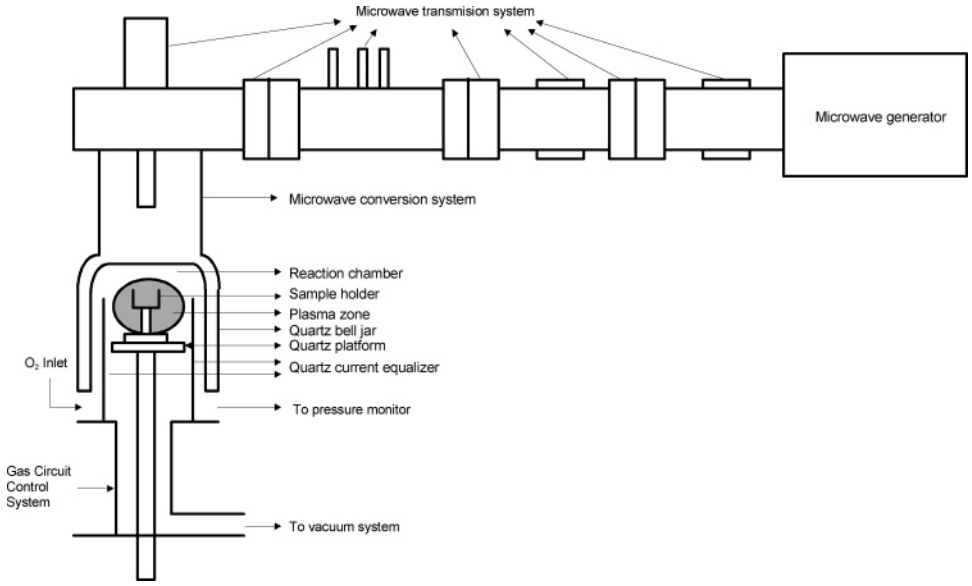

Figure 1. A schematic diagram of microwave plasma equipment.

Table 1. pH Range of Bi^{3+}, Hf^{4+}, and Y^{3+} Metal Ion Precipitation

initial concentration	pH value when precipitation commences	pH value when precipitation ends (residual ion concn < 10^{-14} mol/L)
Bi^{3+} initial concentration (0.075 mol/L)	4.24	8.53
Hf^{4+} initial concentration (0.025 mol/L)	8.4	11.2
Y^{3+} initial concentration (0.025 mol/L)	6.37	10.5

temperature, a nulling technique was necessary to remove any artifacts caused by inductive responses of the test leads and the equipment. The impedance of the leads without a sample was obtained and subtracted from the measurements involving the sample and the electrical leads. The measurements were conducted between 200 °C and 600 °C in ambient atmosphere.

3. Results and Discussion

3.1. Powder Preparation. The uniformity of the powders is significantly influenced by the preparation process and conditions. Since the solubility product of $Bi(OH)_3$, $Hf(OH)_4$, and $Y(OH)_3$ are 4.0×10^{-31}, 4.0×10^{-26}, and 3.2×10^{-26}, respectively,[17] the pH range for the commencement and completion of the precipitation of different metal ions (Bi^{3+}, Hf^{4+}, and Y^{3+}) has been determined separately and is listed in Table 1.

It is well-known that a series of precipitates, such as $BiONO_3$ and $Bi(OH)_3$, can be present simultaneously during the hydrolysis process of $Bi(NO_3)_3$.[11,18,19] It was noticed that during the forward titration process of $Bi(NO_3)_3$ with aqueous ammonia, $BiONO_3$, which could interfere in the successive reactions, was first precipitated, and as a result the final product of the precipitation process was a multiphase mixture of precipitates of Bi^{3+} salts mentioned earlier. Analogously,

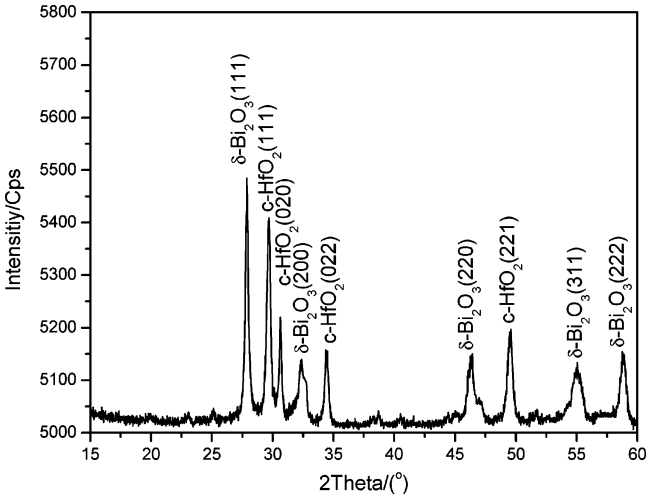

Figure 2. XRD pattern of mixed powder of δ-Bi_2O_3 and c-HfO_2 calcined at 700 °C for 1 h.

$HfO(OH)_2$ precipitates can also be present simultaneously during the hydrolysis process of $HfOCl_2$.[20] Therefore, it was difficult to obtain the pure $Bi(OH)_3$, $Hf(OH)_4$, and $Y(OH)_3$ mixed powders by the forward titration process. In order to overcome this difficulty and obtain pure $Bi(OH)_3$, $Hf(OH)_4$, and $Y(OH)_3$ mixed powders, the reverse chemical titration coprecipitation process was adopted in this research work.[1] In this process, nitrate solution with three metal ions Bi^{3+}, Hf^{4+}, and Y^{3+} was simultaneously titrated with the aqueous ammonia solution having pH ≈ 12 to obtain uniform $Bi(OH)_3$, $Hf(OH)_4$, and $Y(OH)_3$ mixed powders without the formation of $BiONO_3$ and $HfO(OH)_2$. The suitable pH value of aqueous ammonia solution in the reverse chemical titration coprecipitation process was greater than 11.2 from the data presented in Table 1.

X-ray diffraction pattern of mixed hydroxide powders calcined at 700 °C, 1 h is shown in Figure 2. The result indicates that the calcined powder mainly consists of δ-Bi_2O_3

(17) Stephen, H.; Stephen, T. *Solubilities of Inorganic Compounds vol. 1*; Pergamon Press: Oxford, 1963.
(18) Pourbaix, M. Atlas of Electrochemical Equilibria in Aqueous Solutions; Pergamon Press: Oxford, 1966.
(19) He, W. M.; Zhen, Q.; Liu, J. Q.; Pan, Q. Y. *J. Funct. Mater. (Chinese)* **2003**, *34*, 702−706.
(20) Ivanova, E. A.; Konakov, V. G.; Solovyeva, E. N. *Rev. Adv. Mater. Sci.* **2003**, *4*, 41−47.

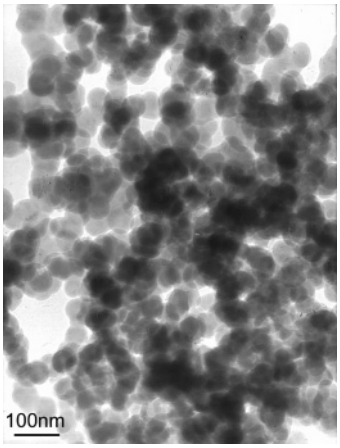

Figure 3. TEM image of nanoparticles of δ-Bi_2O_3 and c-HfO_2 mixed powder after calcining at 700 °C for 1 h.

and c-HfO_2 with only traces of β-Bi_2O_3 (tetragonal) because it is believed that during the calcination process at 700 °C the following solid solution reactions occur between the component oxides:[1]

$$Bi_2O_3 + xY_2O_3 = Bi_2Y_{2x}O_{3+3x} \quad (1)$$

$$HfO_2 + xY_2O_3 = HfY_{2x}O_{2+3x} \quad (2)$$

As a result of the above reactions between Bi_2O_3 and Y_2O_3 as well as HfO_2 and Y_2O_3 the β-Bi_2O_3 (tetragonal) phase transforms into δ-Bi_2O_3 (cubic) and the m-HfO_2 (monoclinic) phase transforms into c-HfO_2 (cubic) with Y_2O_3 acting as a stabilizer. No noticeable residual peaks due to unreacted component oxides could be observed in the XRD trace.

Figure 3 shows the TEM micrograph of the powder after calcination. The particle size of powder was about 40 nm without significant agglomeration as seen in Figure 3. According to the Scherrer formula and from the X-ray diffraction data, the mean diameter of δ-Bi_2O_3 and c-HfO_2 has been found to be approximately 40 and 35 nm, respectively. This is in qualititative agreement with the results shown in the TEM image in Figure 3, suggesting that the particles do not exhibit the tendency of forming agglomerates. Further, the particles of δ-Bi_2O_3 and c-HfO_2 are equiaxed, suggesting that the structure of both the solid solution composition is cubic. It was difficult to determine the exact composition of δ-Bi_2O_3 (cubic) and c-HfO_2 (cubic) with Y_2O_3 acting as a stabilizer due to less than 40 nm grains by EDAX analysis of individual grains, as the spot size of the electron beam in SEM is comparable with the grain size. However, on the basis of the binary T−X phase diagram of Bi_2O_3−Y_2O_3 and HfO_2−Y_2O_3 system reported in the literature and the initial cation concentration reported in Table 1, the concentration of Y_2O_3 in δ-Bi_2O_3 (cubic) and c-HfO_2 (cubic) is estimated as 25 (±2) mol % and 12.5 (±2) mol %, respectively.

3.2. XRD Analysis. The XRD patterns of nanocrystalline solid electrolyte samples synthesized from mixed nanopowders of δ-Bi_2O_3 and c-HfO_2 by the microwave plasma sintering process at 600 °C, 700 °C, and 800 °C for different lengths of sintering time are shown in Figure 4. It is clear from Figure 4 that the major phase constitution of the sintered

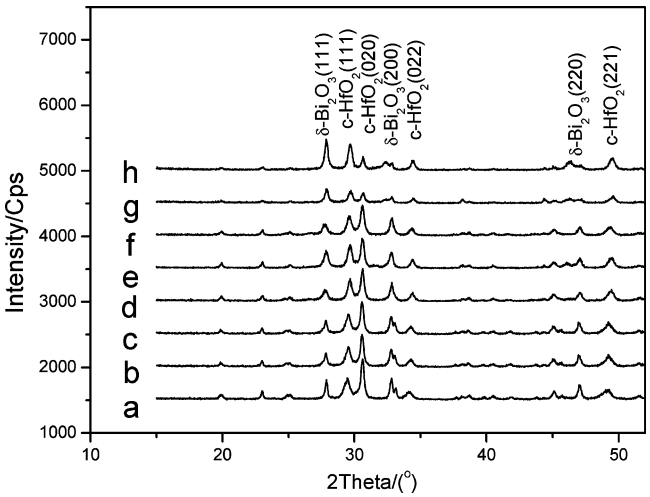

Figure 4. XRD patterns of the samples sintered by using microwave plasma a- 600 °C, 30 min; b- 600 °C, 60 min; c- 700 °C, 5 min; d- 700 °C, 30 min; e- 700 °C, 60 min; f- 800 °C, 5 min; g- 800 °C, 30 min; h- 800 °C, 60 min.

composite material is δ-Bi_2O_3 and c-HfO_2 phases with only traces of β-Bi_2O_3 coexisting during the sintering process. The presence of traces of β-Bi_2O_3 is manifested by the presence of a broad peak around 33° of 2-theta in Figure 2 and in Figure 4. As the temperature and time of sintering is increased, the peak doublet at 33° of 2-theta in Figure 4 also increased in intensity and became a singlet. This in our opinion is due to the transformation of traces of impurity phase consisting of β-Bi_2O_3 to δ-Bi_2O_3. On sintering for 30 min and 60 min at 800 °C, the intensity of the δ-Bi_2O_3 peak at 27.5° of 2-theta increased whereas that at 33° decreased and the peak intensity of c-HfO_2 at 31° of 2-theta decreased too. This is possible due to the partial formation of ternary solid solution between Bi_2O_3−HfO_2−Y_2O_3. Further, the X-ray diffraction peak width at half-maxima diminished with increase in temperature and sintering time because of the slight increase in the grain diameter of δ-Bi_2O_3 and c-HfO_2 grains during the microwave plasma sintering process.

3.3. Grain Growth. The variation of crystallite size of δ-Bi_2O_3 and c-HfO_2 of the nanocrystalline Bi_2O_3−HfO_2−Y_2O_3 solid electrolyte samples sintered by the microwave plasma process as a function of time at 600 °C, 700 °C, and 800 °C is presented in Figure 5 and Figure 6, respectively. It can be seen that the variation of the grain size of both δ-Bi_2O_3 and c-HfO_2 with sintering time follows a parabolic rate law at different sintering temperatures for the samples sintered by the microwave plasma process. It is clear from Figure 5 and Figure 6 that the crystallites grew rapidly in the early sintering stage at 600 °C because both δ-Bi_2O_3 and c-HfO_2 have a high specific surface area in the initial stages of sintering as a result of smaller crystallite size. However, the growth rate reduced as the grain size increased with increase in sintering time. A similar grain growth behavior has been observed at 700 °C for δ-Bi_2O_3 and c-HfO_2, but as expected the rates of grain growth were higher at 700 °C than that at 600 °C for both the solid solution composition. At 800 °C, the rate of grain growth of δ-Bi_2O_3 and c-HfO_2 increased dramatically as seen in Figure 5 and 6, respectively. We believe that this phenomenon is expected as the rate of diffusion of ionic species, and as a result the mass transfer

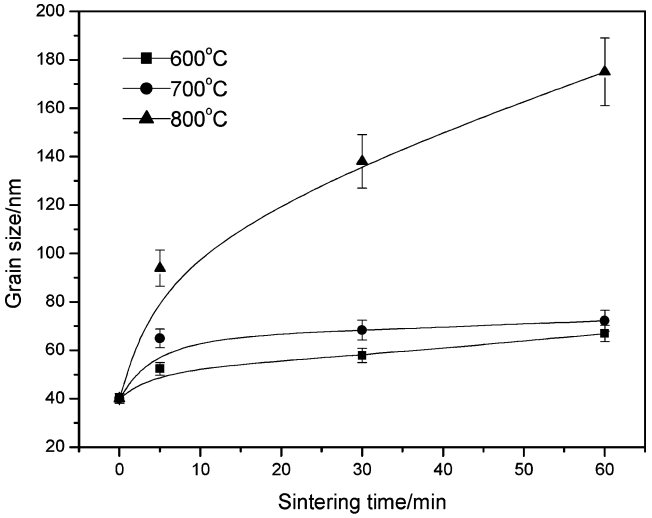

Figure 5. Rate of change of δ-Bi_2O_3 grain size of nanocrystalline Bi_2O_3−HfO_2−Y_2O_3 samples at different temperature during microwave plasma sintering process.

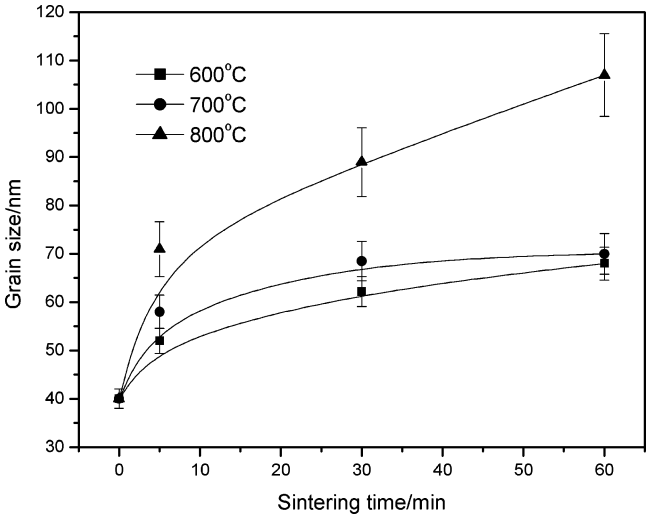

Figure 6. Rate of change of c-HfO_2 grain size of nanocrystalline Bi_2O_3−HfO_2−Y_2O_3 samples at different temperature during microwave plasma sintering process.

across the grain boundaries in the sintered specimens is likely to increase within the solid solution phase as the temperature increases. The interesting point is that there is a window of temperature and time, typically between 600 and 700 °C for 30 to 60 min, within which the grain growth is limited to below 100 nm even though the densification of the sample is greater than 95% for microwave-sintered specimens and greater than 90% for pressureless sintering process as will be seen later.

As a first approximation, the oxide nanoparticles can be considered close to spheres for a cubic solid solution of Bi_2O_3−Y_2O_3 and HfO_2−Y_2O_3. According to the spherical model,[21] the relationship between the variation of grain size ($D - D_0$) in a sintering process, and sintering time (t) at a fixed temperature is given by the expression:

$$(D - D_0)^2 = kt \tag{3}$$

where k is a constant, D is average grain size after sintering, and D_0 is the average initial grain size. Therefore, using the data in Figure 5 and Figure 6, the grain growth in the Bi_2O_3−HfO_2−Y_2O_3 solid solution system at the three different sintering temperatures can be represented by the following equations. The value of D_0 for δ-Bi_2O_3 and c-HfO_2 used in the calculation is 40 and 35 nm, respectively, obtained from the average size of δ-Bi_2O_3 and c-HfO_2 mixed nanopowders calcined at 700 °C for 1 h. Therefore, from the results obtained in this study, the following relationships have been derived at 600, 700, and 800 °C, respectively.

Table 2. Grain Growth Rate Constants (k) of δ-Bi_2O_3 and c-HfO_2

material	600 °C	700 °C	800 °C
δ-Bi_2O_3	11.31	55.99	311.94
c-HfO_2	14.75	30.41	77.43

The following relationships have been obtained at different sintering temperatures for the δ-Bi_2O_3 grains,

$$600\ °C:\ (D - D_0) = 3.36 \times t^{1/2} \tag{4}$$

$$700\ °C:\ (D - D_0) = 4.66 \times t^{1/2} \tag{5}$$

$$800\ °C:\ (D - D_0) = 17.66 \times t^{1/2} \tag{6}$$

and for the c-HfO_2 grains,

$$600\ °C:\ (D - D_0) = 3.83 \times t^{1/2} \tag{7}$$

$$700\ °C:\ (D - D_0) = 4.54 \times t^{1/2} \tag{8}$$

$$800\ °C:\ (D - D_0) = 8.81 \times t^{1/2} \tag{9}$$

Based on the above dynamic equations, the calculated rate constant for the growth of δ-Bi_2O_3 and c-HfO_2 grains as a function of time at three different sintering temperatures is given in Table 2.

According to the Arrhenius equation, the above rate constant (k) in eq 3 can be expressed as a function of the reciprocal of absolute temperature by the expression:

$$k = k_0 \exp\left(\frac{-\Delta E}{R \times T}\right) \tag{10}$$

where k is a rate constant at a fixed temperature of grain growth, k_0 is a preexponential constant at the same temperature, ΔE is a apparent activation energy, R is the universal gas constant, and T is the absolute temperature. Using the data from Table 2, eq 10 yields the apparent activation energy (ΔE) for the growth of nanocrystalline δ-Bi_2O_3 and c-HfO_2 grains to be equal to 125.87 kJ·mol^{-1} and 62.77 kJ·mol^{-1}, respectively within 1% of the uncertainty limits.

The variation of grain size of δ-Bi_2O_3 and c-HfO_2 of the composite nanocrystalline Bi_2O_3−HfO_2−Y_2O_3 solid electrolyte samples sintered by microwave plasma and by pressureless sintering as a function of time at 700 °C is compared in Figure 7 and Figure 8, respectively. It can be seen from Figure 7 and Figure 8 that the rate of grain growth of both δ-Bi_2O_3 and c-HfO_2 using the microwave plasma sintering process is significantly lower compared to that of pressureless sintering.

(21) Kingery, W. D.; Bowen, H. K.; Uhlman, D. R. *Introduction to Ceramics*; John Wiley and Sons Inc.: London 1967.

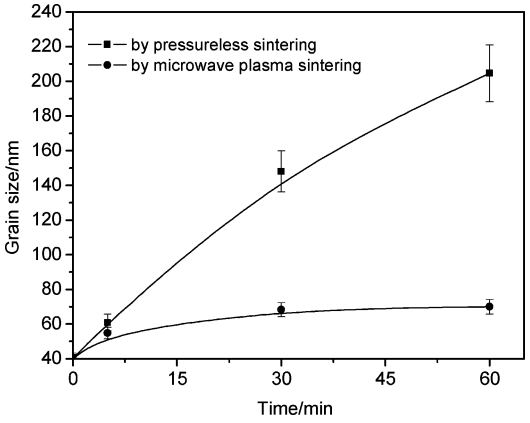

Figure 7. Rate of change of δ-Bi_2O_3 grain size of nanocrystalline $Bi_2O_3-HfO_2-Y_2O_3$ samples at 700 °C by different sintering process.

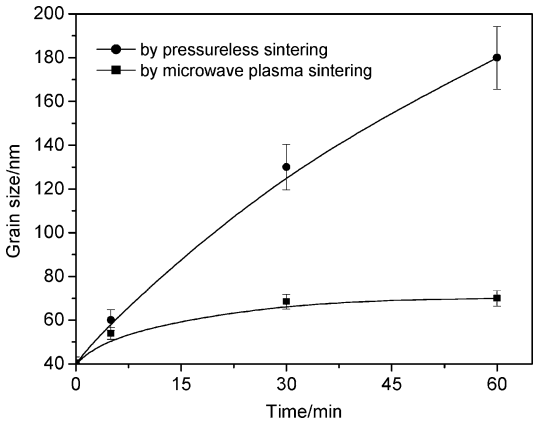

Figure 8. Rate of change of c-HfO_2 grain size of nanocrystalline $Bi_2O_3-HfO_2-Y_2O_3$ samples at 700 °C by different sintering process.

From the results shown in Figures 5−8, it is apparent that the appropriate temperature and time for microwave plasma sintering of nanocrystalline composite solid electrolyte materials made from mixed nanopowders of δ-Bi_2O_3 and c-HfO_2 is probably between 600 and 700 °C for 60 min or more. Under this condition, the grain growth in nanocrystalline $Bi_2O_3-HfO_2-Y_2O_3$ solid electrolyte is at a minimum during the densification process. It is well-known that prevention of excessive grain growth is essential to reap the benefits of nanostructured materials on the physical, electrical, and mechanical properties of the sintered high density solid electrolyte.

3.4. Density Variation. The variation of the relative density of $Bi_2O_3-HfO_2-Y_2O_3$ nanocrystalline samples sintered by microwave plasma and pressureless sintering process as a function of sintering temperature between 600 °C and 800 °C for 30 min is shown in Figure 9. It can be seen from Figure 9 that both processes exhibit a high densification rate probably due to the smaller grain size, high surface area, and smaller diffusion distances. However, at all the three temperatures selected, the relative density of samples sintered by microwave plasma is much higher than that by the pressureless sintering process. This is probably due to the effect of microwave plasma sintering on the rate of diffusion of ions within the ceramic material, enhanced mass transfer at lower temperatures, and improved sintering and grain growth kinetics.[22,23] The nanocrystalline particles have a large surface area, grain boundaries, and a concentration of defects,

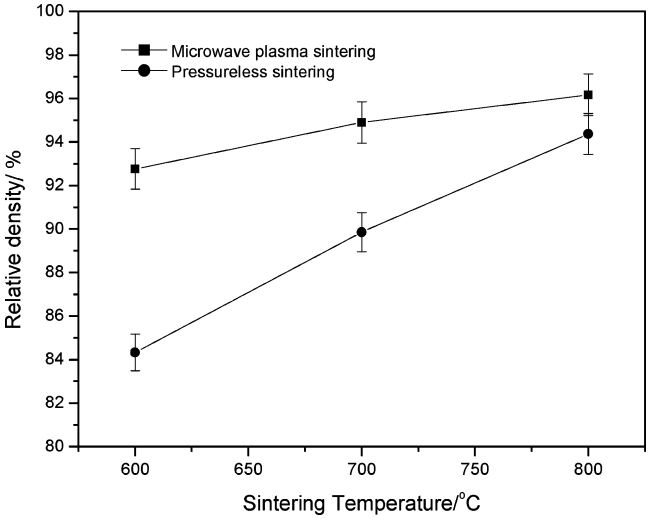

Figure 9. Relative density of $HfO_2-Bi_2O_3-Y_2O_3$ materials by different sintering process in same sintering time of 30 min.

which when coupled with microwave, significantly enhances the diffusion of charged particles (Bi^{3+}, Hf^{4+}, Y^{3+}, and O^{2-}) present in the composite solid electrolyte leading to the enhancement of the rate of sintering processes in the field of microwave plasma. Consequently, the samples having greater than 96% of the relative density could be easily obtained at 700 °C within 30 min of sintering time with negligible grain growth during microwave plasma sintering as shown in Figure 5 and 6 compared to the conventional pressureless sintering process.

3.5. Microstructure. The microstructure at 40 000 magnification of the nanocrystalline $Bi_2O_3-HfO_2-Y_2O_3$ composite solid electrolyte sintered by microwave plasma and by pressureless sintering is shown in Figure 10a and b, respectively. The sample sintered by microwave plasma at 700 °C for 60 min has dense microstructure with a small amount of residual porosity and is virtually crack free as seen in Figure 10a.

However, the sample sintered by the pressureless sintering process at an identical temperature and for the same length of time (700 °C, 60 min) shows that there is significant porosity and has relatively larger grain size, greater than 100 nm, as seen in Figure 10b. From Figure 10a, it can be also seen that both δ-Bi_2O_3 and c-HfO_2 grains have an average size between 60 and 70 nm and have equiaxed morphology, which is excellent for superior mechanical properties such as high fracture toughness and electrical properties such as high ionic conductivity.

3.6. Conductivity. Conductivity of the $Bi_2O_3-HfO_2-Y_2O_3$ composite solid electrolyte sintered by the microwave plasma process at 700 °C over a period of 1 h has been measured using a two-probe AC impedance spectroscopy method. A typical complex impedance diagram at 400 °C is shown in Figure 11. The measured impedance as a function of signal frequency was modeled using commercial software, and the intercept of the arc at lower frequency was treated

(22) Tiegs, T. N.; Kiggams, J. O.; Kimrey, H. D. *Mat. Res. Soc. Symp. Proc.* **1990**, *189*, 243−245.
(23) Janney, M. A.; Kimrey, H. D. *Mat. Res. Soc. Symp. Proc.* **1990**, *189*, 215−217.

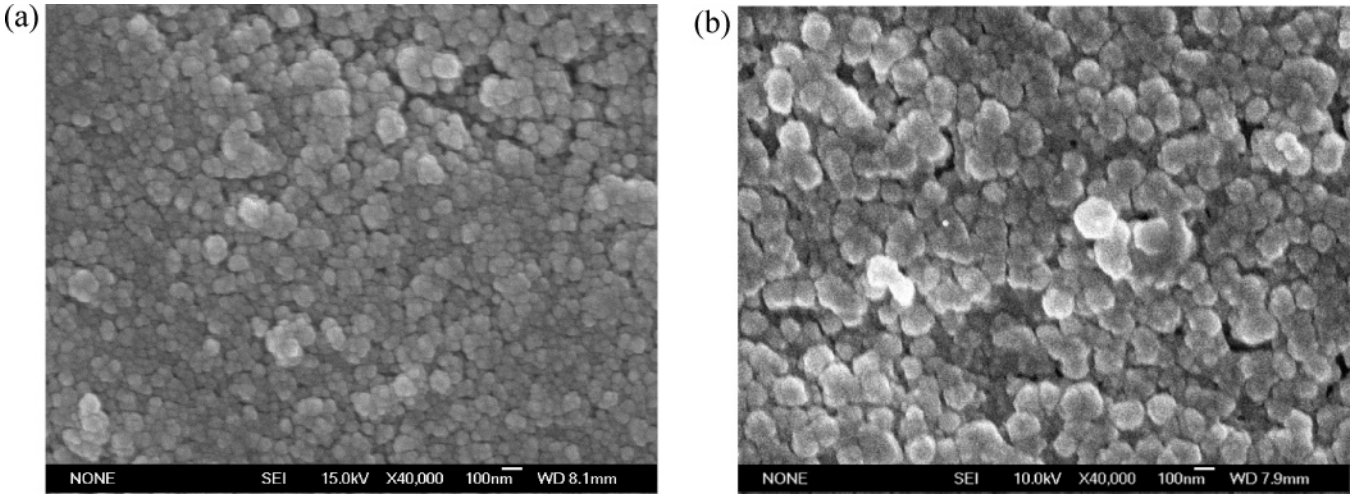

Figure 10. Morphology of $Bi_2O_3-HfO_2-Y_2O_3$ materials by different sintering process. (a) by microwave plasma at 700 °C, 60 min (b) by pressureless sintering at 700 °C, 60 min.

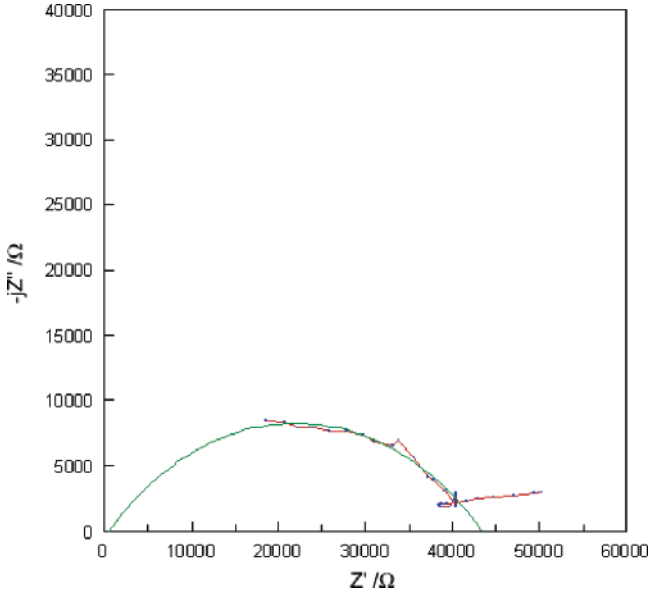

Figure 11. Typical complex impedance diagram of $Bi_2O_3-HfO_2-Y_2O_3$ composite solid electrolyte at 400 °C. The frequency of ac signal increases from right to left in the diagram.

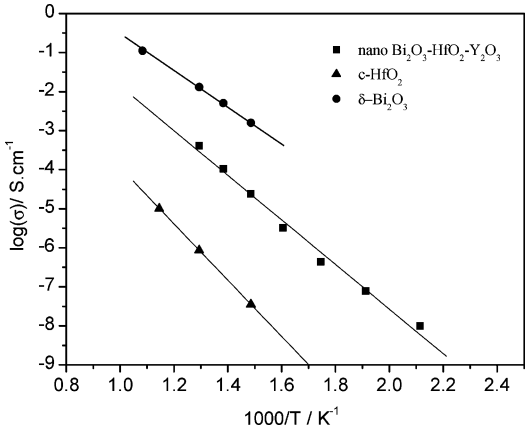

Figure 12. Conductivity of the $Bi_2O_3-HfO_2-Y_2O_3$ and HfO_2-based solid electrolyte materials. The error in the measured data is approximately ±2%.

Table 3. Calculated Grain, Grain Boundary, and Total Conductivity of $Bi_2O_3-HfO_2-Y_2O_3$ Composite Solid Electrolyte from the Complex Impedance Diagrams at Different Temperature of Measurement

temp (°C)	conductivity of grains (σ_b) ($\Omega^{-1}\cdot cm^{-1}$)	conductivity of grain boundary (σ_{gb}) ($\Omega^{-1}\cdot cm^{-1}$)	conductivity of total (σ) ($\Omega^{-1}\cdot cm^{-1}$)
200	5.10×10^{-8}	1.22×10^{-8}	9.86×10^{-9}
250	2.59×10^{-7}	1.10×10^{-7}	7.74×10^{-8}
300	1.65×10^{-6}	5.90×10^{-7}	4.35×10^{-7}
350	6.84×10^{-6}	6.16×10^{-6}	3.24×10^{-6}
400	1.11×10^{-4}	3.02×10^{-5}	2.38×10^{-5}
450	2.32×10^{-4}	1.92×10^{-4}	1.05×10^{-4}
500	2.83×10^{-3}	4.85×10^{-4}	4.14×10^{-4}
550	-	1.10×10^{-2}	1.10×10^{-2}
600	-	6.36×10^{-2}	6.36×10^{-2}

as a measure of impedance of grain and grain boundary whereas the intercept at high frequency was treated as the impedance of grain.

The grain and grain boundary conductivity of the composite nanostructured solid electrolyte at different temperatures computed from the measured impedance data is given in Table 3. The conductivity of nanocrystalline $Bi_2O_3-HfO_2-Y_2O_3$ is compared with the cubic form of microcrystalline $HfO_2-Y_2O_3$ solid electrolyte[24] and the delta form of $(Bi_2O_3)_{0.75}(Y_2O_3)_{0.25}$ solid solution[25] in Figure 12. It can be seen from Figure 12 that the conductivity of nanocrystalline $Bi_2O_3-HfO_2-Y_2O_3$ solid electrolyte obeys an Arrhenius type relationship and is 2 to 4 orders of magnitude higher than that of the microcrystalline HfO_2-based solid electrolyte reported in literature.[24]

Further, from Figure 12 it can be seen that the conductivity of the composite solid electrolyte is approximately 2 orders of magnitude lower than that of δ-Bi_2O_3 consisting of 25 mol%Y_2O_3.[25] This clearly suggests that the nanocrystalline $Bi_2O_3-HfO_2-Y_2O_3$ composite solid electrolyte exhibits average conducting properties compared with the pure $HfO_2-Y_2O_3$ solid electrolyte[24] and $(Bi_2O_3)_{0.75}(Y_2O_3)_{0.25}$ solid solution.[25]

We assume that the composite solid electrolyte material investigated in this study is predominantly an oxygen ion conductor; therefore, the activation energy for oxygen ion (O^{2-}) conduction in $Bi_2O_3-HfO_2-Y_2O_3$ solid electrolyte obtained using the Arrhenius relationship is 1.134 eV, which is less than that of the HfO_2-based microcrystalline solid

(24) Zhuiykouv, S. *J. Euro. Ceram. Soc.* **2000**, *20*, 769−976.
(25) Takahashi, T.; Iwahara, H. *Mater. Res. Bull.* **1978**, *13*, 1447−1453.

electrolyte,[24] 1.431 eV, and very similar to that of δ-$(Bi_2O_3)_{0.75}$-$(Y_2O_3)_{0.25}$ solid solution,[25] 0.87 eV. This suggests that the activation energy for the oxygen ion conduction in the composite solid electrolyte also tends to exhibit an average behavior akin to the conductivity as shown in Figure 12. These values compare reasonably well with the data reported in the literature by Kale et al.[26−28] for ceramic oxide materials bearing similar crystal structure. As a result, the nanocrystalline $Bi_2O_3-HfO_2-Y_2O_3$ electrolyte can be successfully used as an oxide ion conduction membrane in devices such as solid-state gas sensors, low-temperature single chamber SOFC, and oxygen separation membranes. However, this remains to be proved and needs further investigation into the chemical stability of the composite electrolyte in oxygen potential gradients and determination of the ionic conduction domain as a function of temperature and oxygen potentials.

4. Conclusion

In conclusion, mixed nanopowders of δ-Bi_2O_3 and c-HfO_2 were successfully prepared by a reverse chemical titration coprecipitation process using $Bi(NO_3)_3{\cdot}5H_2O$, $HfOCl_2$, and $Y(NO_3)_3{\cdot}6H_2O$ as starting materials and PEG6000 as dispersing agent. After calcination at 700 °C for 60 min, the mixed oxide powders were found to exhibit insignificant agglomeration and were composed of δ-Bi_2O_3 and c-HfO_2 having an average particle size of approximately 40 and 35 nm, respectively. The average composition of Y_2O_3 in δ-Bi_2O_3 is estimated at 25 mol % and that in c-HfO_2 is estimated at 12.5 mol %. The dynamic equations of grain growth obtained in this investigation at the three different temperatures follow the parabolic rate law. Moreover, under microwave plasma sintering conditions, grain growth rate is much lower than that under conventional pressureless sintering. The apparent activation energy for the grain growth (ΔE) of nanocrystalline δ-Bi_2O_3 and c-HfO_2 grains has been found to be 125.87 kJ·mol^{-1} and 62.77 kJ·mol^{-1}, respectively. There is a window of temperature and time, typically between 600 and 700 °C for 30 to 60 min, within which the grain growth is limited to less than 100 nm while the density of the sample is greater than 95% for microwave-sintered specimens relative to 90% for a pressureless sintering process probably because of the greater driving force for sintering of the nanopowders of δ-Bi_2O_3 and c-HfO_2 admixture and possible enhancement of mass transfer within the ceramic compact at lower temperatures due to the coupling of microwave with the cations and anions in the δ-Bi_2O_3 and c-HfO_2 ceramic composite. The conductivity of nanocrystalline $Bi_2O_3-HfO_2-Y_2O_3$ composite solid electrolyte has been found to be an average of the two end members. The activation energy for oxygen ion conduction of $Bi_2O_3-HfO_2-Y_2O_3$ composite solid electrolyte has been found to be 1.134 eV, which is less than that of HfO_2-based solid electrolyte,[24] 1.431 eV, and greater than δ-Bi_2O_3, 0.87 eV.[25]

Acknowledgment. The authors are grateful to the National Natural Science Foundation of China (Grant ref no. 20101006), Nano Technology Special Foundation of Shanghai Science and Technology Committee (Grant ref no.0452 nm073), and Institute for Materials Research at the University of Leeds for supporting this research work.

CM061197I

(26) Kurchania, R.; Kale, G. M. *J. Mater. Res.* **2000**, *15*, 1576−1582.
(27) Wang, L.; Pan, L.; Sun, J.; Hong, Y. R.; Kale, G. M. *J. Mater. Sci.* **2005**, *40*, 1717−1723.
(28) Xiong, W.; Kale, G. M. *Intl. J. Appl. Ceram. Technol.* **2006**, *3*, 210−217.